Preparation of Manganese Ferrite Fine Particles from Aqueous Solution

Z. X. TANG,* C. M. SORENSEN,*,[1] K. J. KLABUNDE,†
AND G. C. HADJIPANAYIS‡

*Department of Physics and †Department of Chemistry, Kansas State University, Manhattan, Kansas 66506; and
‡Department of Physics and Astronomy, University of Delaware, Newark, Delaware 19716

Received September 17, 1990; accepted March 1, 1991

Fine manganese ferrite particles have been prepared by a coprecipitation method and subsequent digestion process (below 100°C). Manganous salts mixed with either ferric or ferrous salts were coprecipitated with sodium hydroxide. Particles produced from ferric salts were $MnFe_2O_4$ with relatively smaller sizes (5 to 25 nm) while ferrous salts created $Mn_xFe_{3-x}O_4$ ($0.2 < x < 0.7$) with bigger sizes up to 180 nm. In either case, the particle size appeared to be a unique function of the ratio of metal ion concentration to hydroxide ion concentration when the digestion conditions were fixed. For the system with ferric salts, the undigested samples were polycrystals with crystallite sizes of about 2 nm. Digestion, which could be described as an Ostwald ripening process, did not change the crystalline structure but increased both the crystallite size and the particle size. A basic solution was essential for an effective digestion process in this system. The system with ferrous salts, on the contrary, needed an acidic solution to create a single ferrite phase. Digestion changed both the crystalline structure and the particle size of the precipitated precursors. This process involved a dissolution and renucleation/growth mechanism. Cation and anion effects on the particle size and the evolution during digestion were also studied.

I. INTRODUCTION

In the course of studying the magnetic properties of fine particles, particle size is among the most important parameters. Therefore, it is desirable to develop the ability to prepare particles which span a large size range and yet retain uniformity among other important qualities such as composition, crystallinity, and morphology. The coprecipitation of metallic ions followed by an appropriate digestion (aging) process offered a potential technique for this purpose.

Coprecipitation has been used for many investigations on ferrites. The preparation processes fall into two main categories. Both use metallic salts as the starting compounds and hydroxides (KOH, NaOH, NH_4OH, etc.) as the reaction agents, followed by digestion (aging). The difference lies in the selection of the starting iron compounds. The first category uses the ferric (Fe(III)) salts. With the divalent ions being one or two of Mn, Fe, Co, Ni, or Zn, corresponding ferrites have been successfully produced (1, 2). From these studies, it has been found that pH values and digestion temperatures and times affect the particle size and morphology, but few details have been given. The second method uses ferrous (Fe(II)) salts and divalent salts as the starting materials, with KNO_3 as an oxidizing agent (3–9).

In this work, we prepared manganese ferrite fine particles of different sizes (5 to 180 nm) from aqueous solutions with either ferric or ferrous salts as the starting materials. Macroscopically, we controlled the particle size by adjusting the ratio of metal salt to hydroxide concentration. Microscopically, detailed investigations on the evolution from the undigested precursors to the final ferrites were performed.

[1] To whom correspondence should be addressed.

0021-9797/91 $3.00

II. EXPERIMENTAL METHODS

All starting materials were reagent purity and used without further purification. Water used in solution and washing was distilled and deionized. Two types of precipitation processes were performed.

(1) Prepare solutions of the sodium hydroxide (NaOH) and the metal (Fe(III) and Mn(II)) salts. For example, in one 250-ml beaker was placed a 100-ml solution in which 6.00 g NaOH was dissolved in water. In another 250-ml beaker, 2.70 g $FeCl_3 \cdot 6H_2O$ and 0.99 g $MnCl_2 \cdot 4H_2O$ were dissolved in water to produce a 50-ml solution. The atomic ratio of Mn(II) to Fe(III) was 0.5. The metal salt solution was slowly poured into the solution of sodium hydroxide, which led to precipitation. The system was continuously stirred by a magnetic stirrer during mixing. This process was varied so that the total molarity of the metal ions calculated for the final solution volume covered a range of 0.015 to 0.25 *M*. That of the hydroxide was from 0.50 to 2.5 *M*.

(2) Similar to (1), only replace Fe(III) with Fe(II). In this case, potassium nitrate (KNO_3) was added to the NaOH solution as an oxidation agent with a fixed concentration of 0.25 *M* in the final solution. The molarity of the metal ions was adjusted between 0.05 and 0.35 *M*. That of the hydroxide ranged from 0.33 to 1.00 *M*.

After mixing the solutions to cause precipitation, the beaker which contained the precipitant was brought into a preheated bath of water and ethylene glycol for digestion. We varied digestion time and temperature (below 100°C). A mechanical stirrer was inserted into the solution during digestion. It stirred slowly to create an uniform temperature and mixture in the solution without causing vigorous agitation. Suspensions (both digested and undigested) were repeatedly washed with water and filtered using ashless filter paper before drying at about 50°C to a powder. The following techniques were used to characterize the particle properties and to monitor the chemical reaction processes.

(1) X-ray diffraction. A Scintag X-ray diffractometer was used to identify the intermediate phases and the final spinel ferrite phases. The $K\alpha$ line of Cu was its radiation.

(2) Transmission electron microscope. We ultrasonically dispersed powder samples into ethanol. Drops of the dispersion were dropped onto carbon-coated copper grids for investigation.

(3) BET measurement. This technique measures the surface area by the Brunauer, Emmett, and Teller method. If we know the bulk density and suppose a particle shape, particle size can be calculated from the surface area. Even though the particles may not be perfectly spherical or cubic as usually assumed, the dimensional size will not differ too much from the real mean size, provided that the surface is smooth and no pores exist in the particles.

(4) pH meter. We used an Orion Research pH meter (Ionalyzer/Model 407A) to measure the pH values for different solutions and the pH value changes during digestion.

(5) Mössbauer spectroscopy. The Mössbauer spectra were recorded at room temperature in the conventional transmission geometry by an MS-1200 Mössbauer spectrometer (Ranger Scientific, Inc.). The source was ^{57}Co embedded in a rhodium matrix. We reported the isomer shift (δ) relative to pure iron.

(6) Chemical analysis. Mn was determined colorimetrically by oxidation of Mn(II) to the highly colored permanganate ion. Absorption was measured at 525 nm. A few samples were also analysed for their Fe content using atomic absorption/emission spectroscopy.

III. RESULTS AND DISCUSSION

The experimental steps followed our motivation to change the particle size as much as possible. First of all, we studied the $FeCl_3$ + $MnCl_2$ + NaOH system. This system resulted in small sizes. Second, we searched for systems leading to bigger particle sizes by in-

vestigating the effect of changing the anion and cation. Third, the system of $FeSO_4$ + $MnCl_2$ + KNO_3 + NaOH was chosen to prepare larger particles. For the first and third systems, phase evolution during digestion has been studied in detail.

1. $FeCl_3$ + $MnCl_2$ + NaOH System

(1) Comparison of Undigested and Digested Samples

The undigested sample showed broad peaks in X-ray diffraction as seen in Fig. 1a; the same sample showed sharp $MnFe_2O_4$ peaks after digestion at 100°C for 90 min (Fig. 1b). The pH values before and after digestion were 12.5. In spite of broad peaks, the positions and intensities of the diffraction peaks in Fig. 1a coincided exactly with those on $MnFe_2O_4$ in Fig. 1b, if we consider that one apparent broad peak may include more than one diffraction peak. The broad peaks were caused by the very small crystallite size. Using the Scherrer formula (10), the crystallite size was estimated to be about 2 nm for the undigested sample and greater than 5 nm for the digested one.

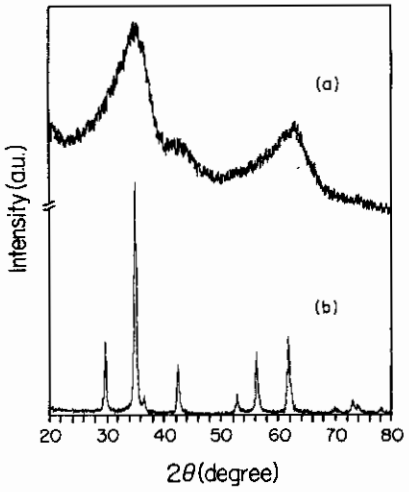

FIG. 1. X-ray diffraction patterns for an undigested sample (a) and a digested sample (b) for the $FeCl_3$ + $MnCl_2$ + NaOH system. Digestion: 100°C and 90 min. For both samples, $[Fe^{+3}] + [Mn^{+2}] = 0.1\ M$ with $[Mn^{+2}]/[Fe^{+3}] = 0.5$ and $[OH^-] = 0.5\ M$.

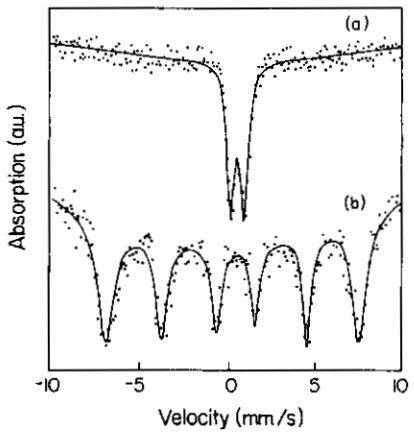

FIG. 2. Mössbauer effect spectra for the undigested sample (a) and the digested sample (b) in Fig. 1. The points are the experimental data and the solid lines are the fitted spectra.

Compared with the bulk lattice constant for $MnFe_2O_4$ of 0.85 nm, the crystallite size of 2 nm is only on the order of a few lattice planes.

Since the X-ray diffraction pattern of the undigested sample was so broad, it is valuable to substantiate the presence of the ferrite phase by another independent technique. We used Mössbauer spectroscopy to perform further investigation, since the parameters of the Mössbauer effect, in contrast to X-ray diffraction, depend on mainly the nearest-neighbor environment, not on the long-range order periodicity. Two Mössbauer spectra are shown in Fig. 2, where spectra (a) and (b) correspond to the undigested and digested samples in Fig. 1, respectively. We fitted spectrum (a) in Fig. 2 with a doublet and spectrum (b) with a sextet. The fitted parameters are listed in Table I. It was also possible to fit curve (b) with two sextets, corresponding to Fe ions in two different sites, the tetrahedral and octahedral sites in the ferrite, since the linewidths from the one sextet fitting were not symmetric about the spectrum center. Nevertheless, we list only the results of the one sextet fitting because of the small differences between the two sites.

The isomer shift and internal magnetic field for the sextet were consistent with those of manganese ferrite (11, 12), which supported

TABLE I

Hyperfine Mössbauer Effect Parameters for an Undigested (Doublet) and a Digested (Sextet) Sample ($FeCl_3$ + $MnCl_2$ + NaOH System)

	$\lvert\Delta E\rvert$ (mm/s)	δ (mm/s)	H (kOe)
Doublet	0.75 (2)	0.40 (2)	0
Sextet	0.10 (2)	0.33 (2)	466
Manganese ferrite (11, 12)	≈0	0.41	468

Note. Numbers in the brackets are the errors for the last digit.

the conclusion of the X-ray diffraction measurements. For the undigested sample, it might be reasonable to assign the doublet as a collapsed magnetic ferrite phase because of possible superparamagnetic behavior at room temperature. To support this conjecture we first note that the doublet had the same isomer shift as $MnFe_2O_4$, implying that the short-range electrostatic interaction was of the ferrite type. Second, if a bulk anisotropy constant 4.0×10^4 J m^{-3} (13) and the lifetime of the excited γ-photon (10^{-7} s for the ^{57}Co source) are used, the calculated superparamagnetic size of $MnFe_2O_4$ is about 10 nm. This could be the upper limit if the anisotropy constant of the fine particles was higher than the bulk one due to the surface effects. Pannaparayil *et al.* (14) did record a superparamagnetic Mössbauer spectrum at 238 K for 9.8-nm $NiFe_2O_4$ particles. The bulk anisotropy constant of $NiFe_2O_4$ is 6.7×10^4 J m^{-3} (13), which is close to that of $MnFe_2O_4$. Therefore, it is reasonable that our 2-nm $MnFe_2O_4$ particles are superparamagnetic at room temperature. As for the difference of our quadrupole splitting from that of the references, it can be attributed to the atoms in the asymmetric environment on the grain boundary (or particle surfaces) which may dominate due to the small crystallite size. This effect was much more enhanced in the undigested sample.

Chemical analysis revealed that the undigested and digested samples had the Mn/Fe atomic ratio of 0.52 and 0.53, respectively, close to the correct ratio of 0.5 for $MnFe_2O_4$. Thus we conclude that both the undigested and digested products were stoichiometric manganese ferrite ($MnFe_2O_4$), the undigested sample having a very small crystallite size.

(2) General Results

Digestion was performed at 100°C for 90 min. This temperature could cause quick digestion so that 90 min was long enough to reach the equilibrium particle size and yet was still below the boiling point of the suspensions. In calcualting d_{BET} (particle diameter measured by the BET method), a spherical particle shape was assumed and the bulk density of $MnFe_2O_4$ (5.0 g/cm^3) (15) was used. Different curves were obtained corresponding to different hydroxide ion concentrations if we plotted the d_{BET} of the digested samples as a function of the total molarity of the metal ions [Me] which is the sum of [Fe^{+3}] and [Mn^{+2}]. Sizes of the digested particles in a fixed [OH^-] concentration increased almost linearly with the increasing of metal ion concentration, except for a few points. The slopes of these linear relations were functions of the hydroxide concentration. These curves could be reduced to a universal curve by replotting as a function of [Me]/[OH^-] only, as shown by the open symbols in Fig. 3. Particle size increased with

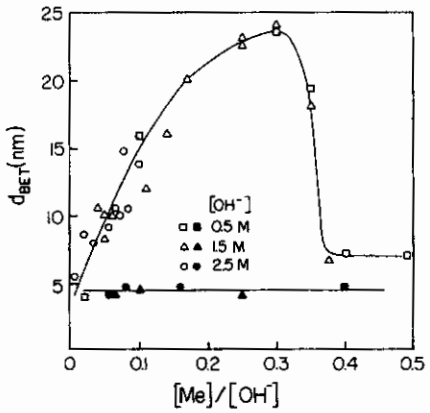

FIG. 3. Particle size as a function of the [Me]/[OH^-] ratio for the $FeCl_3$ + $MnCl_2$ + NaOH system, where [Me] is the sum of [Fe^{+3}] and [Mn^{+2}]. Solid symbols: before digestion. Open symbols: after digestion at 100°C for 90 min.

the increasing ratio up to $[Me]/[OH^-] = 0.3$, after which the size decreased with $[Me]/[OH^-]$ until reaching a constant only slightly larger than the undigested size for samples with $[Me]/[OH^-] > 0.375$. Crystallite sizes determined by Scherrer's formula (10) using the half-maximum width of the (311) X-ray diffraction line were consistent with d_{BET}, indicating the single crystal character of these digested particles. For the undigested samples, on the other hand, particle size kept constant despite the different starting conditions. Comparing the smaller crystallite size (~2 nm) with the bigger particle size ($d_{BET} \sim 4$ nm), the polycrystalline nature of the undigested samples was revealed.

Thus we see that two regions separated by $[Me]/[OH^-] = 0.375$ exist. For $[Me]/[OH^-] < 0.375$, digestion takes small, polycrystalline $MnFe_2O_4$ and produces larger, single-crystal particles with size controllable up to 25 nm. For $[Me]/[OH^-] > 0.375$, digestion has little effect on particle size. However, the phase is always $MnFe_2O_4$ regardless of the initial conditions or digestion treatment.

(3) Evolution during Digestion

Very interesting aspects of the digestion appeared when we studied the time evolution of the precipitate. Figure 4 shows some X-ray diffraction patterns in this process. For example, after digestion at 100°C for 5 min, the X-ray diffraction (Fig. 4b) appeared to be a superposition of two patterns, both belonging to the ferrite phase, except having different crystallite sizes. Similar diffraction patterns were also obtained for other digestion temperatures (Figs. 4e and 4f). One pattern is still broad, similar to that of the undigested sample, but on top of those broad peaks stand much sharper diffraction peaks with crystallite sizes greater than 5 nm. As the digestion time increased, the broad spectrum diminished and the sharp peaks grew in intensity, indicating a discrete, bimodal transformation of small crystallites to larger ones, as seen in Figs. 4a–f for a variety of times and temperatures. This

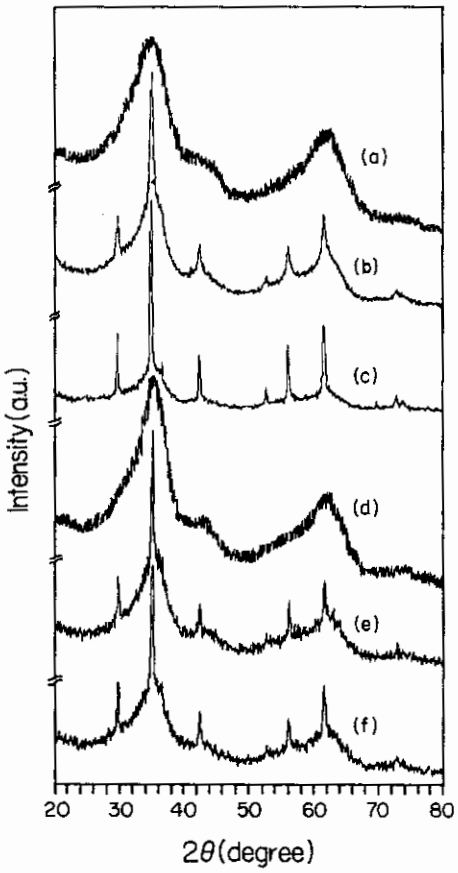

FIG. 4. X-ray diffraction patterns for samples of $[Me]/[OH^-] = 0.1$ ($FeCl_3 + MnCl_2 + NaOH$ system) which were digested at different temperatures and different times. (a) Undigested, (b) 100°C, 5 min, (c) 90°C, 40 min, (d) 70°C, 20 min, (e) 70°C, 40 min, and (f) 50°C, 100 min.

raised questions concerning why the crystallite size did not change continuously and what kind of process brought this type of evolution about during digestion. Further experimentation was performed to help us understand this transformation process.

(a) The activation energy of the digestion process was determined by the following procedures. For a fixed digestion temperature, a series of samples with different digestion times were prepared. These samples were investigated by X-ray diffraction in the order of increasing digestion time. The digestion time (t_d) at which the new larger crystallite size ap-

peared was taken as the time between the times for which the sample still showed broad X-ray diffraction peaks (Fig. 4d as an example) and the time when the sample first showed the bimodal X-ray diffraction pattern, as in Fig. 4e. We plot these results in Fig. 5 for four different digestion temperatures. The straight line indicates an Arrhenius behavior, with an activation energy derived from the slope of 25kJ/mol. This energy is smaller than the typical bond enthalpy (16), suggesting that no bond-breaking processes are involved in the digestion process.

(b) A sintering mechanism was ruled out. After annealing the undigested dry powder samples up to 480°C in Ar gas for 1 h, no sharp diffraction pattern was observed; instead the broad pattern persisted. Therefore the sintering mechanism is probably not applicable because of the much lower digestion temperature we had used to affect a change in solution.

(c) The precipitate must be digested in the presence of a perceivable amount of OH^- ions (a basic solution with a high enough pH value) in order to have an effective digestion to cause crystallite and overall BET sizes. In addition to the aforementioned examples of $[Me]/[OH^-] > 0.375$ (Fig. 3), other evidence was obtained. For example, after precipitating from a solution of pH 13 (corresponding to $[Me]/[OH^-] = 0.01$), the undigested precursor was repeatedly washed until the pH value of the solution was close to 7.0. Digestion of this suspension did not create any new X-ray diffraction patterns; the broad pattern endured.

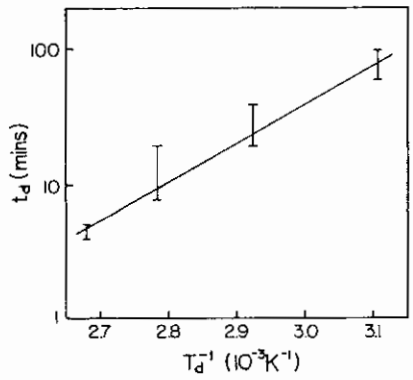

FIG. 5. The digestion time (t_d) needed to bring about the sharp X-ray diffraction pattern as a function of the reciprocal digestion temperature (T_d^{-1}) for the $FeCl_3 + MnCl_2 + NaOH$ system.

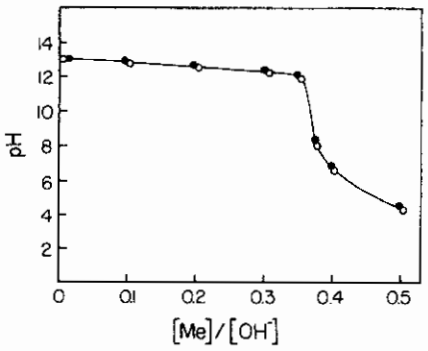

FIG. 6. pH value changes with the $[Me]/[OH^-]$ ratio for the $FeCl_3 + MnCl_2 + NaOH$ system, where [Me] is the total concentration of metal ions. Solid and open circles are the results before and after digestion, respectively. Digestion: 100°C and 90 min.

(d) While the pH value changed with $[Me]/[OH^-]$, it was not changed by digestion (Fig. 6). This supported a digestion without bond breaking, since bond breaking might involve absorption or release of OH^- or H^+.

(4) Discussion

Without phase changing, without sintering, and without bond breaking, the digestion process might be properly described as an Ostwald ripening process (17), in which the ions dissolve from the smaller crystals and are deposited on the bigger ones, resulting in a growth of the bigger crystals at the expense of the smaller ones. The lower activation energy was probably due to the dissolution energy in the basic solution. Nevertheless, occurrence of the Ostwald ripening is conditional.

All initial mixtures of metal salts and NaOH, regardless of the value of $[Me]/[OH^-]$, create the same small crystallite size particles of $MnFe_2O_4$. The resulting supernatant solutions, however, were different. The Ostwald ripening hypothesis can be further supported by considering the following as-

sumed reactions: For $x > 8([Me]/[OH^-] < 0.375)$,

$$MnCl_2 + 2FeCl_3 + x\text{NaOH} \rightarrow MnFe_2O_4 + (x - 8)\text{NaOH} + 4H_2O + 8\text{NaCl}. \quad [1]$$

The resulting solution is basic with excess OH^- ions. For $x < 8([Me]/[OH^-] > 0.375)$,

$$MnCl_2 + 2FeCl_3 + x\text{NaOH} \rightarrow \frac{x}{8} MnFe_2O_4 + \left(1 - \frac{x}{8}\right)(MnCl_2 + 2FeCl_3) + \frac{x}{2} H_2O + x\text{NaCl}. \quad [2]$$

The solution has excess metal ions. Both expressions lead to the same equation at $x = 8([Me]/[OH^-] = 0.375)$,

$$MnCl_2 + 2FeCl_3 + 8\text{NaOH} \rightarrow MnFe_2O_4 + 4H_2O + 8\text{NaCl}. \quad [3]$$

In view of Eqs. [1]–[3], we propose a mechanism in which OH^- acts as a catalyst in an Ostwald ripening process. For $x > 8$ $([Me]/[OH^-] < 0.375)$ there is excess OH^- in the solution and pH > 8.5. When a $MnFe_2O_4$ "molecule" dissolves, Mn^{+2}, Fe^{+3}, and $O^{-2} \rightarrow OH^-$ ions are formed. The Fe^{+3} and Mn^{+2} ions react with the large concentration of OH^- to reprecipitate on the larger, and thermodynamically more stable, particles. For $x < 8$ $([Me]/[OH^-] > 0.375)$, pH < 8.5. A pH of 9 or greater is necessary to cause precipitation of Mn in this system (see below); hence the metal ions have a significantly reduced tendency to reprecipitate. The rapid change of pH through this region makes for a rapid change in the digestion properties as well.

The equilibrium size of the particles after digestion may be related to the particle surface charge determined by the absorbed ions. The Paneth–Fajans rule (18) states that the ions that will be strongly absorbed are those which form sparingly soluble or weakly dissociated compounds with the oppositely charged ions of the solid lattice. Hence it is reasonable to propose that our solid particles adsorb OH^- ions to become negatively charged, more so with higher OH^- ion concentration. A positively charged counterion layer would then form and the potential across this layer could control transport of ions to the particle, leading to an equilibrium size. The higher the surface charge density, the smaller the equilibrium size. The size in Fig. 3 and the pH value in Fig. 6 do change in the right direction with $[Me]/[OH^-]$ to support the size increase with this ratio for $[Me]/[OH^-] \leq 0.3$. Finally, we suggest that the bimodal size distribution during digestion may be a geometric behavior of the polycrystalline undigested particles. The proposed Ostwald ripening would operate on the outer layer crystallites first, dissolving them and transforming them to bigger ones. The inner cyrstallites, on the other hand, remain unattracted during the early stages of the process. This would explain the superimposed X-ray diffraction patterns at the early stage of the digestion.

2. Cation and Anion Effects on Particle Size

In an attempt to prepare larger particles, we prepared samples with different cations and anions. Table II lists the resulting particle sizes (d_{BET}) after digestion. Although experiments with both excess metal ions and excess hydroxide ions have been carried out, only those leading to well-crystallized ferrites as confirmed by X-ray diffraction are tabulated. For

TABLE II

Particle Sizes d_{BET} (nm) after Digestion for Different Cation and Anion Systems, where $[Me]/[OH^-] = 0.3$ for the Ferric Systems and $[Me^{+2}]/[OH^-] = 0.6$ for the Ferrous Systems

	$MnCl_2$	$MnSO_4$	$CoCl_2$
$FeCl_3$	23.4		9.7
$Fe(NO_3)_3$	20.5	12.8	
$Fe_2(SO_4)_3$	10.5[a]		
$FeSO_4$	100.9	121.0	115.2

Note. All samples were digested at 100°C for 90 min.
[a] $[Me]/[OH^-] = 0.1$.

TABLE III

Some Oxidation Potentials (21) Involving NO_3^- and SO_4^{-2}

Reactions	Potential (V)
$Fe^{+2} = Fe^{+3} + e^-$	−0.77
$2NO_3^- + 4H^+ + 2e^- = 2H_2O + N_2O_4$	+0.81
$NO_3^- + 3H^+ + 2e^- = H_2O + HNO_2$	+0.94
$NO_3^- + 4H^+ + 3e^- = 2H_2O + NO$	+0.96
$SO_4^{-2} + 4H^+ + 2e^- = H_2O + H_2SO_4$	+0.20
$2SO_4^{-2} + 4H^+ + 2e^- = 2H_2O + S_2O_6^{-2}$	+0.20

the ferric system, $[Me]/[OH^-]$ was chosen as 0.3, at which we obtained the biggest particle size in the $FeCl_3 + MnCl_2 + NaOH$ system. We chose $[Me^{+2}]/[OH^-] = 0.6$, where $[Me^{+2}]$ is the sum of the metal ions, for the ferrous system because early works (5, 6) had concluded that a small excess of metal ions was needed in order to create the larger particle sizes for Ni and Co ferrites. An exception to these selections was the $Fe_2(SO_4)_3 + MnCl_2 + NaOH$ system, for which particles prepared at $[Me]/[OH^-] = 0.3$ were not ferrite. Instead, we used $[Me]/[OH^-] = 0.1$ in order to obtain the ferrite particles for this case. Here one of the anions (SO_4^{-2}) was divalent. The enhanced shielding due to this divalent anion may have prevented the cations from coming together, or the sulfate ion's known complexing behavior with the ferric ion (19, 20) may have affected this reaction.

From this table, it is clear that anions have but a minor effect on particle size. Cations at the same oxidation state (e.g., Mn(II) and Co(II)) do not increase particle size either. The big increase in size occurred when the oxidation state of the iron cations change from Fe(III) to Fe(II). Therefore, we chose Fe^{+2} and Mn^{+2} as the system for our further studies.

3. $FeSO_4 + MnCl_2 + KNO_3 + NaOH$ System

This system was more complicate than the ferric case because the oxidation states of the starting materials were not the same as those of the final product. Iron was in the +2 state in $FeSO_4$ and must be oxidized to the +3 state of the ferrite, hence the need for NO_3^{-1} as an oxidation agent. Experiments confirmed the necessity of NO_3^{-1} without which the final product was nonferrite. Table III lists the oxidation potentials of different reactions (21). Since the oxidation of Fe(II) to Fe(III) needs a potential of 0.77 V, only those reactions which could accept electrons and supply 0.77 V or more can behave as an oxidation agent in this reaction. NO_3^{-1} satisfies this requirement, whereas SO_4^{-2} does not.

(1) Particle Size Profile

Particle size d_{BET} was a function of $[Me^{+2}]$ (i.e., $[Fe^{+2}] + [Mn^{+2}]$). Two curves for the digested samples corresponding to $[OH^-]$ of 0.33 and 0.50 *M* were obtained. The digestion temperature and time were selected as 100°C and 90 min for the same reasons as those given for the ferric system. Once again, the data collapse to a single curve of d_{BET} vs $[Me^{+2}]/[OH^-]$ (Fig. 7). The particle sizes of a few undigested samples are also shown in Fig. 7 by the solid squares. All calculations of d_{BET} used the density of the bulk $MnFe_2O_4$, which

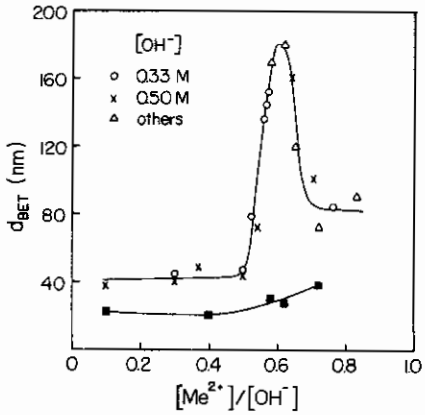

FIG. 7. Particle size as a function of the ratio of the metal ion concentration to the hydroxide ion concentration $[Me^{+2}]/[OH^-]$ for the $FeSO_4 + MnCl_2 + KNO_3 + NaOH$ system, where $[Me^{+2}] = [Mn^{+2}] + [Fe^{+2}]$. The open symbols are for the samples after digestion at 100°C for 90 min. The solid squares show the sizes of some undigested samples.

TABLE IV

Phases of the Undigested Samples and Mn Contents after Digestion for the $FeSO_4 + MnCl_2 + KNO_3 + NaOH$ System, $[Me^{+2}] = [Fe^{+2}] + [Mn^{+2}]$

$[Me^{+2}]/[OH^-]$	0.1	0.6	0.8
Phases	$\delta - (Fe_{0.67}Mn_{0.33})OOH$ and ferrite	Green rust[a]	Green rust[a] and $\beta - FeOOH$
Mn (wt%)	20.1	16.6	4.9

Note. The stoichiometric Mn content for $MnFe_2O_4$ is 23.8 wt%.
[a] Mn substituted green rust (see text).

made the size for those nonferrite samples useful only in a relative sense. The particle size d_{BET} after digestion vs $[Me^{+2}]/[OH^-]$ showed a nonmonotonic behavior with an enhanced change around $[Me^{+2}]/[OH^-] = 0.6$, while the sizes of the undigested samples remained unchanged.

(2) Undigested Samples

Unlike the ferric system, the ferrous system created several crystalline phases before digestion. Table IV shows some X-ray diffraction results for the undigested samples. Also shown are the manganese contents after digestion. Among them, the phase called "green rust" needs a special description and we use the term to imply some uncertainties. X-ray diffraction data of this phase did not fit any known powder diffraction file, but they were close to those of some green rusts. Bernal, Dasgupta, and Mackay (22) studied X-ray diffraction of some green rusts, such as $Fe^{+2}_{3.6}Fe^{+3}_{0.9}(O, OH, Cl)_9$, $Fe^{+2}_{0.36}Fe^{+3}_{0.9}(O, OH, SO_4)_9$, and $Fe^{+2}_{3.6}Fe^{+3}_{0.4}(O, OH, Br)_9$, all with hexagonal structures. They used reactions similar to ours. For example, they formed $Fe^{+2}_{3.6}Fe^{+3}_{0.9}(O, OH, Cl)_9$ from chloride solution by the addition of insufficient alkali to precipitate all Fe^{+2} under oxygen-free conditions, followed by bubbling air through the suspension. In table V we compared their X-ray diffraction data with ours. The two green rusts listed differ only in one of the anions, from Cl^- to SO_4^{-2}, yet their lattice constants a_0 differed by 7.5%. The lattice constants of our green rust calculated from the separations between lattice planes (23) by the assumed indices were $a_0 = 3.70$ Å and $c_0 = 25.9$Å, 7.0 and 14.0%, respectively, from those of $Fe^{+2}_{0.9}(O, OH, Cl)_9$. In addition to the anion influence, the cation Mn^{+2} present in our particles must also have affected the lattice constants of our green rust. Hence our green rust was probably a Mn-substituted green rust.

(3) Digested Samples

The simplest chemical reactions among the metal ions and the hydroxide ions can be written as

$$Fe^{+2} + 2OH^- \rightarrow Fe(OH)_2 \qquad [4]$$

TABLE V

Main Peak Positions (Å) on X-Ray Diffraction for Green Rusts

Index (*hkl*)	$Fe^{+2}_{3.6}Fe^{+3}_{0.9}(O, OH, Cl)_9$ (a_0 = 24.2 Å, c_0 = 3.198 Å)	$Fe^{+2}_{1.6}Fe^{+3}_{0.8}(O, OH, SO_4)_9$ (a_0 = 22.5 Å, c_0 = 3.23 Å)	Our green rust (a_0 = 25.9 Å, c_0 = 3.70 Å)
003	8.02	7.49	8.59
006	4.01	3.84	4.35
012	2.701	2.72	3.01
015	2.408	2.47	2.80

$$Mn^{+2} + 2OH^- \rightarrow Mn(OH)_2, \quad [5]$$

where $[Me^{+2}]/[OH^-] = 0.5$ in these reactions. Thus we divide our experiment into two regions.

A. $[Me^{+2}]/[OH^-] < 0.5$. This was the region in which there was excess OH^-, i.e., $\frac{1}{2}[OH^-] - [Me^{+2}] > 0$. There was a coexistence of the spinel ferrite and the hexagonal $\delta - (Fe_{0.67}Mn_{0.33})OOH$ for both undigested and digested samples. Digestion converted the hexagonal phase to the ferrite. Usually, this conversion was not complete. The closer the $[Me^{+2}]/[OH^-]$ was to 0.5, the more conversion the digestion created. At $[Me^{+2}]/[OH^-] = 0.5$, only a trace of $\delta - (Fe_{0.67}Mn_{0.33})OOH$ could be found by X-ray diffraction after digestion for 90 min at 100°C.

B. $[Me^{+2}]/[OH^-] > 0.5$. Unlike the other region, this one was more complex in that:

(a) The relationship between particle size and $[Me^{+2}]/[OH^-]$ was nonmonotonic; a sharp peak at $[Me^{+2}]/[OH^-] = 0.6$ was followed by a plateau (see Fig. 7).

(b) Although all digested samples were made up of the spinel ferrite as revealed by X-ray diffraction, the Mn/Fe atomic ratios were not as close to 0.5 as they should be in $MnFe_2O_4$. Instead, $Mn_xFe_{3-x}O_4$ was produced according to the Mn contents in Table IV, where x was 0.7 at $[Me^{+2}]/[OH_-] = 0.6$ and x was only 0.2 at $[Me^{+2}]/[OH^-] = 0.8$.

The changes in pH with digestion for the above two regions were not the same (Fig. 8). For $[Me^{+2}]/[OH^-] < 0.5$, pH values were the same before and after digestion. Reasons for this lack of change were that most of the Fe^{+2} ions were already oxidized to Fe^{+3} before digestion (in $\delta - (Fe_{0.67}Mn_{0.33})OOH$ and the ferrite phase) and that the high concentration of OH^- ions, which made the solution insensitive to small OH^-, changes. The decrease of the pH value with digestion for $[Me^{+2}]/[OH^-] > 0.5$ was caused by the oxidation of Fe^{+2} ions. Before digestion in the green rust phase, only a small fraction of iron ions was oxidized. Most of them were oxidized during digestion. The reactions (4) which lead to the formation of magnetite particles under similar conditions can be used with minor substitution. Here we rewrite only one of them as an example.

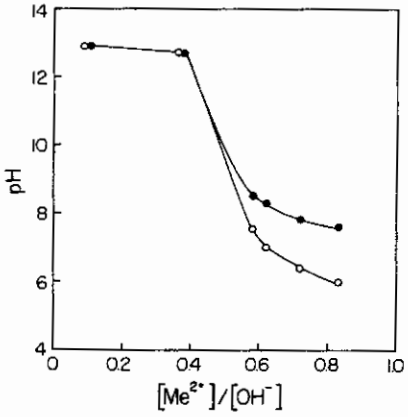

FIG. 8. pH values before (solid circles) and after (open circles) digestion for the $FeSO_4 + MnCl_2 + KNO_3 + NaOH$ system. Digestion: 100°C and 90 min.

$$2Fe^{+2} + Mn^{+2}\,NO_3^- + 3H_2O \rightarrow MnFe_2O_4 + NO_3^- + 6H^+ \quad [6]$$

This reaction releases H^+, which can explain the pH decrease.

(4) Phase Evolution at $[Me^{+2}]/[OH^-] = 0.6$

This was the ratio at which we obtained the maximum particle size. A careful study of the phase evolution during digestion was performed. Figure 9 illustrates the TEM pictures taken at different digestion times (t_d) when the temperature was held at 100°C. Corresponding X-ray diffraction patterns are shown on Fig. 10. The broad peak at about $2\theta = 13°$ comes from the diffraction by the plastic sample holder. For $t_d = 0$ (undigested case), particles were small and poorly defined (Fig. 9a); a Mn-substituted green rust phase was determined by X-ray diffraction (Fig. 10a). After digestion for 5 min, particles in the TEM picture were still predominately the same as those in the undigested case but a few hexagonal

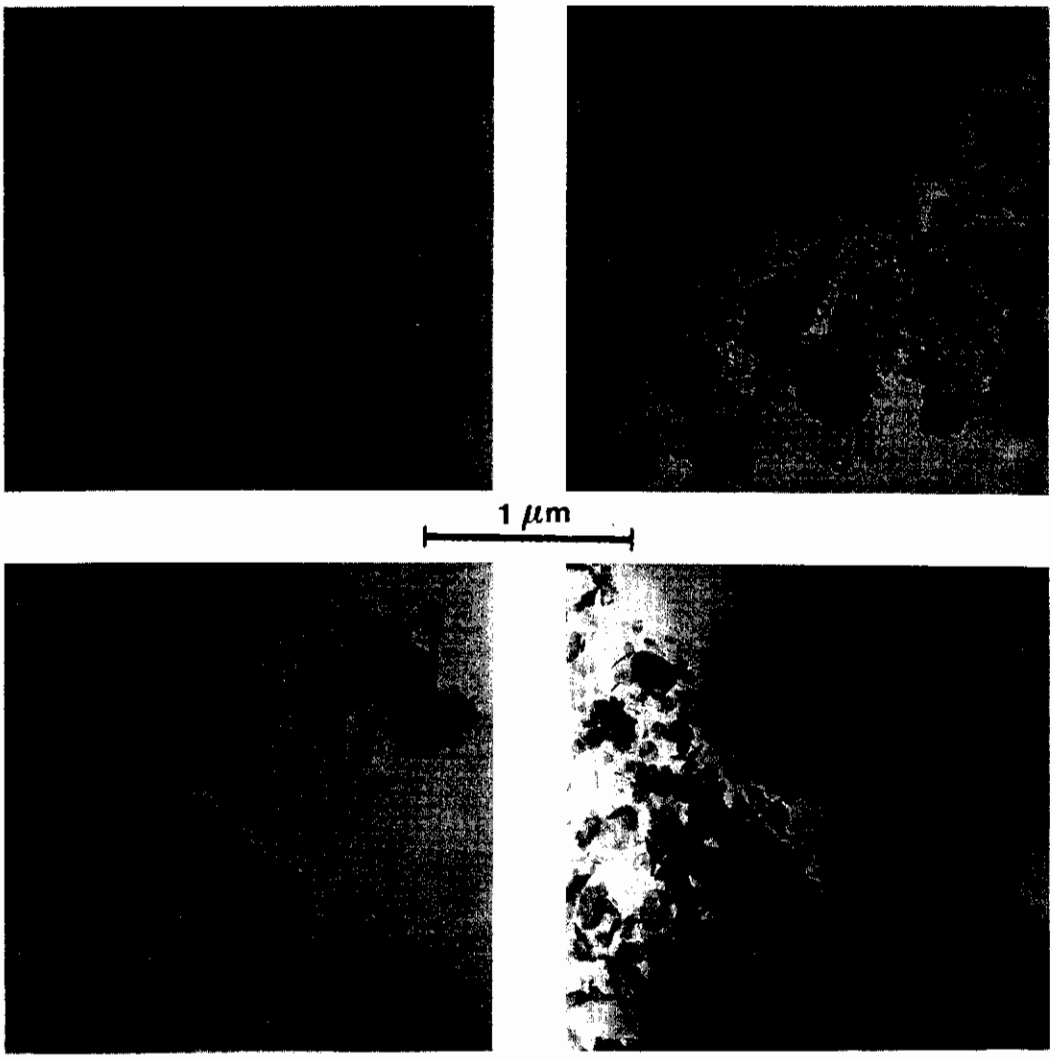

FIG. 9. TEM pictures taken at different digestion times for samples of the $FeSO_4$ + $MnCl_2$ + KNO_3 + NaOH system digested at 100°C. $[Me^{+2}]/[OH^-] = 0.6$. (a) Undigested, (b) 5 min, (c) 10 min, (d) 15 min, (e) 20 min, (f) 40 min, (g) 90 min, and (h) 180 min.

particles appeared in Fig. 9b. Figure 10b also reflects this change by a few new diffraction peaks, as marked by "H". This phase developed clearly to a hexagonal $Fe_2O_3 \cdot H_2O$ (Figs. 9c and 10c). Chemical reactions related to the oxidation of Fe^{+2} to Fe^{+3} must also accompany these changes. The short time needed to cause this transformation indicates the low stability of green rust. When the digestion time increased to 15 min, we found a few small spherical particles in the TEM picture (Fig. 9d), and concomitant with this morphological change the diffraction pattern of the ferrite appeared, as indicated by "F" (ferrite) in Fig. 10d). After that, the spherical particles grew at the expense of the hexagonal phase. At t_d = 40 min, only spherical particles and a trace of hexagonal plates remained (Fig. 9f). X-ray

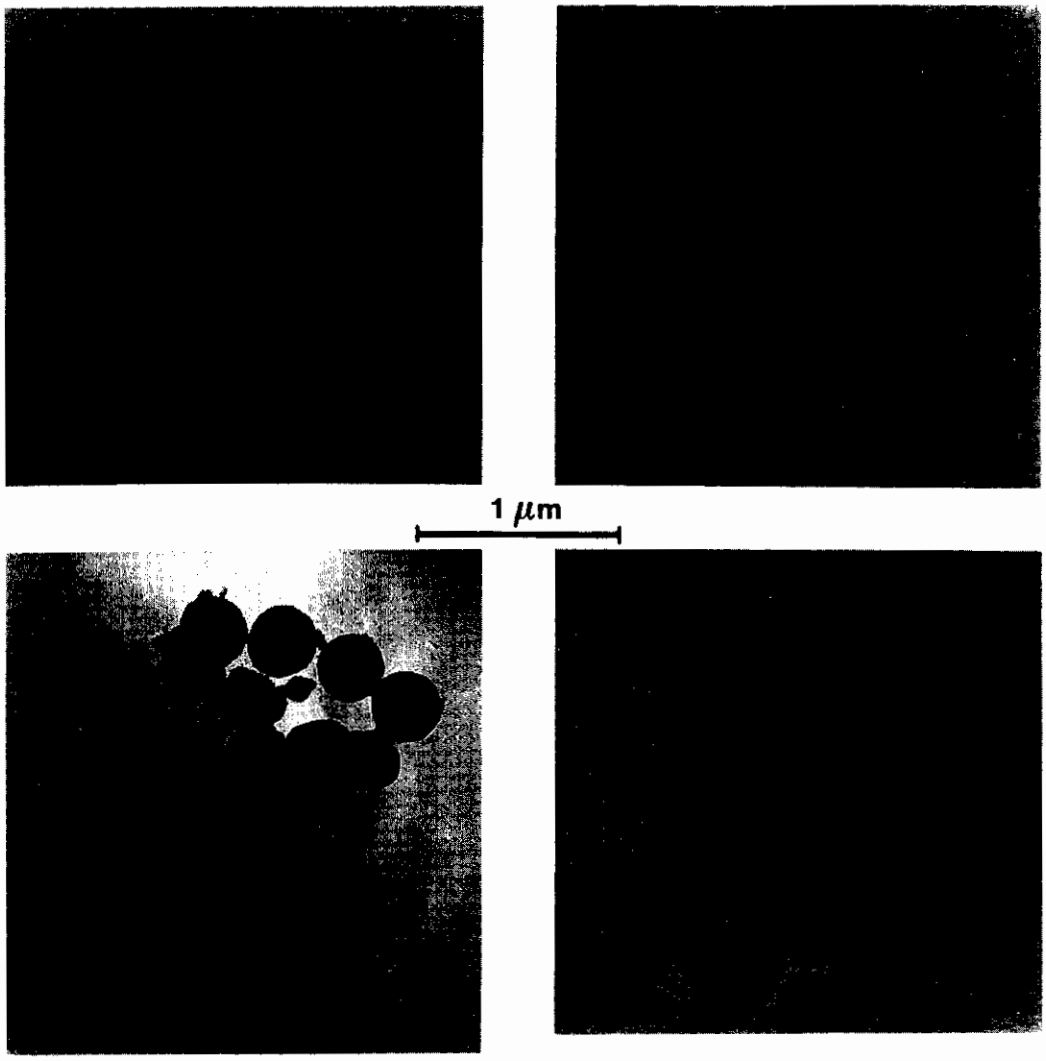

FIG. 9—*Continued*

diffraction showed only the ferrite phase (Fig. 10f). Digestion for longer than 90 min made the particles only more uniform. Figure 9h (t_d = 180 min) gave us very uniform spherical particles. Figure 11 shows the specific surface area and manganese contents for the above evolution. The stoichiometric Mn content for $MnFe_2O_4$ is 23.8 wt%. It is evident that both quantities started an enhanced change only after the appearance of the ferrite phase in Figs. 9d and 10d at t_d = 15 min.

(5) Discussion

The size profile in Fig. 7 is similar to many others; a small excess of metal ions was required to produce uniform spherical ferrite particles (4–6). The above TEM pictures are good evidence that dissolution and renucleation/growth occurred from $Fe_2O_3 \cdot H_2O$ to the ferrite during digestion. This was different in the $Fe^{+2} - Fe^{+3}$ system (4), where a coagulation mechanism or a contact-recrystalliza-

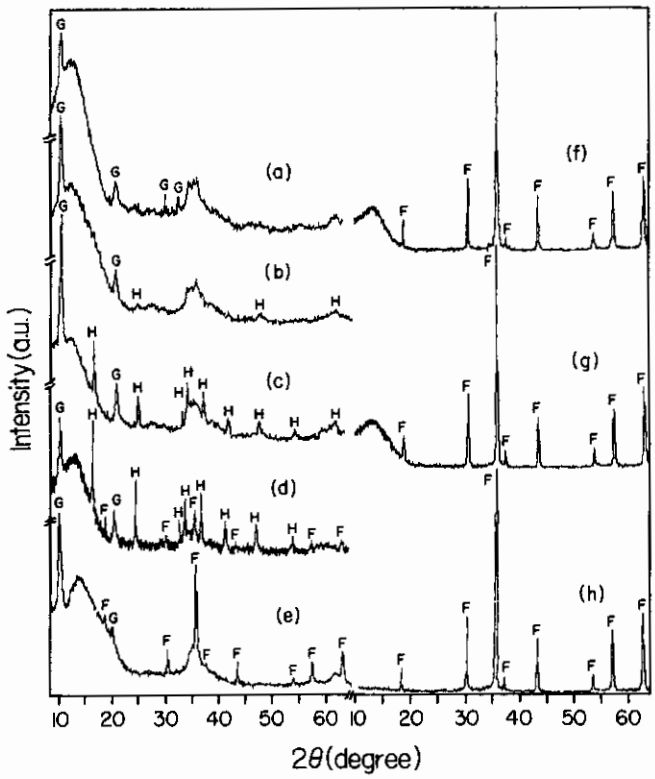

FIG. 10. X-ray diffraction patterns for the $FeSO_4 + MnCl_2 + KNO_3 + NaOH$ system with $[Me^{+2}]/[OH^-] = 0.6$ digested at 100°C for different times. (a) Undigested, (b) 5 min, (c) 10 min, (d) 15 min, (e) 20 min, (f) 40 min, (g) 90 min, and (h) 180 min. The letters "G", "H", and "F" denote Mn-substituted "green rust", hydrated iron oxide $Fe_2O_3 \cdot H_2O$, and ferrite, respectively. The broad peak around $2\theta = 13°$ is the diffraction from the plastic sample holder.

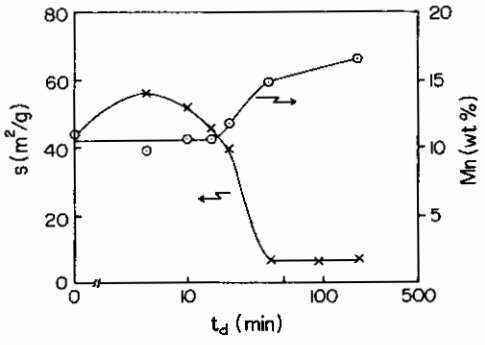

FIG. 11. Specific surface area (s) and manganese content change with digestion time (t_d) for the $FeSO_4 + MnCl_2 + KNO_3 + MaOH$ system with $[Me^{+2}]/[OH^-] = 0.6$ digested at 100°C.

tion mechanism was involved in the formation of the large spheres.

Earlier work (3–6) appears to show that pure ferrites with Me/Fe = 0.5, where Me was a divalent element, could not be obtained by the digestion of green rust, with the exception of magnetite. Authors in Ref. (5) succeeded in explaining the relative enrichments of Co^{+2}, Ni^{+2}, and Mg^{+2} in their ferrites by the free energy changes calculated on the basis of an assumed reaction. We would like to look at this problem from an experimental point of view. The precipitation of hydrous oxides can be initiated from aqueous solution only above certain pH values (24). Table VI lists those

TABLE VI

The Minimum pH Values (pH_{min}) Required to Precipitate Metal Hydroxides when a Single Cation Was Used, and The Maximum $(Me/Fe)_{max}$ Obtained for the Corresponding Ferrites when the Metal Divalent and Fe(II) Cation Were Used in the Coprecipitation Technique, where Me Stands for the Listed Divalent Metal Ions

Metal ion	pH_{min}	$(Me/Fe)_{max}$ (Reference)
Mg(II)	11	0.1 (3)
Mn(II)	9	0.3 (This work)
Ni(II)	8	0.36 (5)
Co(II)	8	0.5 (6)
Fe(II)	7	0.5 (4)
Fe(III)	3	

minimum pH values (pH_{min}) when a single cation was used to precipitate the corresponding metal hydroxide, and $(Me/Fe)_{max}$ which is the maximum Me/Fe ratio in the corresponding ferrites prepared by digesting the coprecipitated product of the divalent metal ion and Fe(II). Fe(III) is listed for comparison. The Me/Fe ratio in the particles increases when the pH_{min} declines to that of Fe(II). Furthermore we propose that the reason for this correlation is that the closer the two pH_{min} were, the easier they could precipitate simultaneously. Note that in the $FeCl_3 + MnCl_2 + NaOH$ system, because of the high pH solution we used, no partial precipitations are involved for Fe(III) and Mn(II). Further experiments need to be done and should include the initial and final pH values before and after digestion.

This argument can also explain the smaller Mn/Fe ratio (0.1) at $[Me^{+2}]/[OH^-] = 0.8$ compared with that at $[Me^{+2}]/[OH^-] = 0.6$, where Mn/Fe = 0.3, since the pH value of the solution was much closer to the pH_{min} of Mn for the latter.

IV. SUMMARY

From our studies, the following conclusions can be drawn.

1. Coprecipitation of the metal ions and the the subsequent digestion (aging) process are a proper technique to produce magnetic ferrite with a wide range of particle sizes.

2. Systems including ferric and manganous chlorides created small stoichiometric $MnFe_2O_4$ particles with size controllable between 5 and 25 nm. The digestion process was effective only in basic solution and could be described by an Ostwald ripening.

3. Anions had but minor effects on particle size. Cations at the same oxidation states did not significantly modify the particle size, while the change of the cation's oxidation states had a strong influence on the particle size.

4. The ferrous and manganous salt system produced bigger ferrite particles (above 50 nm). The products were $Mn_xFe_{3-x}O_4$ with $x < 0.7$. The single ferrite phase could be prepared only in acidic solution. A dissolution and renucleation/growth could be clearly seen from TEM pictures during digestion.

5. The particle size appeared to be a unique function of the ratio of metal ion concentration to hydroxide ion concentration when the digestion conditions were fixed.

ACKNOWLEDGMENTS

This work was supported by NSF Grant CHE-8706954. We thank Dr. G. Glavee and Miss K. Easam for their assistance in obtaining Mössbauer spectra and chemical analyses. ZXT thanks Dr. J. F. Merklin for helpful discussions.

REFERENCES

1. Sato, T., *IEEE Trans. Magn.* **6,** 795 (1970).
2. Sato, T., Hjima, T., Seki, M., and Inagaki, N., *J. Magn. Magn. Mater.* **65,** 252 (1987).
3. Kaneko, K., and Katsura, T., *Bull. Chem. Soc. Jpn.* **52,** 747 (1979).
4. Sugimoto, T., and Matijević, E., *J. Colloid Interface Sci.* **74,** 227 (1980).
5. Regazzoni, T., and Matijević, E., *Corrosion* **38,** 212 (1982).
6. Tamura, H., and Matijević, E., *J. Colloid Interface Sci.* **90,** 100 (1982).
7. Matijević, E., Simpson, C. M., Amin, N., and Arajs, S., *Colloids Surf.* **21,** 101 (1986).
8. Matijević, E., *J. Colloid Interface Sci.* **117,** 593 (1987).
9. Fan, X.-J., and Matijević, E., *J. Am. Ceram. Soc.* **71,** C-60 (1988).

10. Cullity, B. D., "Elements of X-Ray Diffraction," p. 102. Addison–Wesley, London, 1978.
11. Hrynkiewicz, A. Z., Kulgawczuk, D. S., and Tomala, K., *Acta Phys. Pol.* **28,** 423 (1965).
12. Belov, V. F., Devisheva, M. N., Zheludev, I. S., Makarov, E. E., Stukan, R. A., and Trukhtanov, V. A., *Sov. Phys. Solid State (Engl. Transl.)* **6,** 2747 (1965).
13. Chen, C.-W., "Magnetism and Metallurgy of Soft Magnetic Materials," p. 211. North-Holland, New York, 1977.
14. Pannaparayil, T., Marande, R., Komarneni, S., and Sankar, S. G., *J. Appl. Phys.* **64,** 5641 (1988).
15. Cullity, B. D., "Introduction to Magnetic Materials," p. 190. Addison–Wesley, London, 1972.
16. Atkins, P. W., "Physical Chemistry," p. 111. Freeman, San Francisco, 1978.
17. Chernov, A. A., "Modern Crystallography III: Crystal Growth." Springer-Verlag, Berlin, 1984.
18. Skoog, D. A., and West, D. M., "Fundamentals of Analytical Chemistry," p. 167. Holt, Rinehart & Winston, New York, 1963.
19. Sapieszko, R. S., Patel, R. C., and Matijević, E., *J. Phys. Chem.* **81,** 1061 (1977).
20. Matijević, E., Sapieszko, R. S., and Melville, J. B., *J. Colloid Interface Sci.* **50,** 567 (1975).
21. Latime, W. M., "The Oxidation States of the Elements and Their Potentials in Aqueous Solutions," p. 294. Prentice–Hall, New York, 1938.
22. JCPDS, "Powder Diffraction File," 13-88, 13-90, and 13-91. International Centre for Diffraction Data, Swarthmore, PA, 1986.
23. Warren, B. E., "X-Ray Diffraction," p. 21. Addison–Wesley, London, 1969.
24. Skoog, D. A., and West, D. M., "Fundamentals of Analytical Chemistry," p. 746. Holt, Rinehart & Winston, New York, 1963.